The Egyptian Journal of Hospital Medicine (January 2023) Vol. 90, Page 308-320

Therapeutic Role of Salivary Exosomes in Improving Histological and Biochemical Changes Induced by Duct Ligation in the Submandibular Glands of Albino Rats

Nahla E. Ibrahem[1], Noura H. Mekawy[1], Samia Hussein*[2], Heba M. Abdel-aziz[1]
Departments of [1]Medical Histology and Cell Biology and [2]Medical Biochemistry and Molecular Biology, Faculty of Medicine, Zagazig University, Egypt
***Corresponding author:** Samia Hussein, **Mobile:** (+20) 01062725981, **E-Mail:** samiahussein82@hotmail.com

ABSTRACT

Background: Salivary gland diseases are induced by radiotherapy, autoimmune diseases, inflammation, trauma, and obstructive lesions. They result in functional gland impairment which harms oral health and quality of life. Exosomes are extracellular nanoparticles produced by a variety of cells including stem cells. Exosomes facilitate the paracrine functions of the releasing cells, and they are easily absorbed and can integrate with target cells resulting in long-lasting effects. **Objective:** To identify the therapeutic role of exosomes in the histological and biochemical changes in the submandibular gland (SMG) of adult male albino rats after duct ligation.

Materials and methods: Forty adult male albino rats were included in this study. They were distributed in three main groups: control, duct-ligated and treated groups. Exosomes were isolated from the saliva of healthy rats. The treated group received salivary exosomes one week after duct ligation. At the end of the study, the SMG was removed from all groups and two samples were obtained from each gland: one for antioxidant measurement and RNA extraction with subsequent gene expression determination. The other was used for histopathological and immunohistochemical analysis.

Results: The ligated group revealed degenerative histological changes including vacuolated cytoplasm, apoptotic nuclei, congested blood vessels and cellular infiltrate. Increased area percentage of both collagen fibers and S100 immunoreactivity was detected. The treated group showed an amelioration in the histological and immunohistochemical picture. After treatment with exosomes, a significant increase in all antioxidants was recorded. This was accompanied by an increase in both c-kit and cytokeratin-5 gene expression.

Conclusion: There were improved histological, immunohistochemical and biochemical alterations after treatment with salivary exosomes. So, salivary exosomes could be a possible modality in treating SMG diseases.

Keywords: Therapeutic Role of Salivary Exosomes, Duct Ligation in the Submandibular Glands, Albino Rats.

INTRODUCTION

Salivary glands have an important role in maintaining the general health of the oral tissues by saliva. Saliva aids in digestion, enamel protection, lubrication and pH buffering. Additionally, it has anti-inflammatory, anti-bacterial and anti-fungal properties. About 60% of saliva is secreted by the second-largest salivary gland, the submandibular gland (SMG) [1].

Radiotherapy, autoimmune disease, inflammation and trauma to the salivary gland and obstruction of the gland duct by calculi are all known to cause diseases of the salivary gland [2]. Duct ligation is a helpful experimental strategy for examining the mechanisms behind salivary gland inflammation and regeneration since the SMG can improve after inflammatory and fibrotic changes caused by ligation [3].

Exosomes are extracellular nanoparticles. They have a lipid bilayer with a diameter range from 30 to 150 nanometers, and they are secreted by several cells, including stem cells. Their composition reflects the composition of the parental cells and they facilitate the paracrine functions of the releasing cells. They are stable and relatively difficult to degrade. Also, they are easily absorbed and can integrate with target cells resulting in long-lasting effects [4].

Exosomes are present in many body fluids including saliva. They transport lipids, RNAs, and proteins. They are also active carriers for target protein delivery driving genetic and epigenetic changes and contributing to organ crosstalk. Exosomes have been used in clinical trials to diagnose or cure a variety of disorders and understand their pathogenesis [5].

S100 protein family members are multifunctional proteins that interact with several effector proteins in the cells. They control secretion, protein phosphorylation and synthesis, cell division, cell growth and differentiation, transcription and protection from oxidative cell damage. S100 protein is mainly found in some neurons, glial and Schwann cells of normal nervous tissues. Also, its expression was reported in oligodendrocytes and adipocytes. Antibodies to the S100 protein are signs of salivary gland cellular damage [6]. Current treatments for salivary gland diseases are palliative. Thus, how to effectively reverse atrophy and recover the function of the salivary gland is an urgent issue. So, this study was performed to clarify the therapeutic role of exosomes in the structural and biochemical alterations in the SMG of adult male albino rats following duct ligation.

MATERIAL AND METHOD

Study design:

In our study, 40 healthy adult male albino rats of weight 150–200g on average were included. Rats were grown in sterile conditions (23±5° and 12 hours of darkness and light cycles). They were given a standard pellet diet and an access to water. All rats received human care in compliance with the guidelines of the

Received: 22/08/2022
Accepted: 23/10/2022

Medical Research Ethics Committee of Zagazig University, Egypt (ZU-IACUC/3/F/235/2022) and conformed to the National Institutes of Health guide for the care and use of laboratory animals.

Animals were distributed in three groups:

Group I (control): Twenty-four healthy rats. They were equally distributed in three subgroups.

Subgroup (Ia): eight rats were not subjected to any procedure.

Subgroup (Ib): eight rats were subjected to a sham operation under anesthesia using sodium pentobarbital (50mg/kg IP). A midline skin incision was made in the neck. Then, the main excretory duct of the SMG identification and manipulation without ligation were made.

Subgroup (Ic): eight rats received 0.2mL phosphate-buffered saline (PBS) (vehicle for salivary exosomes) by intravenous injection, once per day for four weeks starting from the beginning of the 2nd week of the study.

Group II (SMG-ligated group): eight rats were exposed to ligation of the main excretory duct of the right SMG leaving the gland on the left side non-ligated. It was performed under general anesthesia (sodium pentobarbital, 50mg/kg IP). Each rat stayed in the supine position and a midline skin incision was made in the neck. The main excretory duct of the right SMG was displayed by detaching peripheral tissues such as nerves and blood vessels, with care taken not to harm them. The duct was ligated nearly 2mm above the salivary gland using a 4-0 silk suture and the wound was closed [7]. After seven days, two animals were sacrificed to confirm the structural changes induced by duct ligation. Five weeks after duct ligation, the rest of the rats were sacrificed (at the end of the experiment).

Group III (Exosome-treated group): eight rats were subjected to SMG duct ligation as in group II. After seven days, the rats received salivary exosomes by intravenous injection in the tail vein (100µg/kg/dose suspended in 0.2mL PBS) once per day for four weeks [8].

Five weeks after duct ligation (at the end of the experiment), the rats were sacrificed and the SMGs were removed. Two parts of each SMG were collected for analysis: one preserved at -80^{0}C for homogenization using a power homogenizer with subsequent biochemical measurement and molecular study. The other part was preserved for histopathological and immunohistochemical analysis.

Extraction of salivary exosomes

Saliva from healthy rats was centrifuged at 2,000×*g* for 10min at room temperature to remove cells and debris. Then, 0.5mL of the clarified supernatant was diluted with 0.5mL of PBS. After that, 0.5mL of Total Exosome Isolation reagent (From other body fluids) (Invitrogen) was added. The tube was vortexed until the solution was homogenous. After incubation at 4ºC for one hour, the sample was centrifuged at 10000×*g* for one hour in a cooling centrifuge at 4ºC. The formed pellet was resuspended in 50µL PBS and characterized by transmission electron microscopy (TEM) and using FACS, including CD9, CD63, and CD11b surface expression.

Transmission electron microscopy (TEM)

The exosomes were suspended in a solution of 2.5% glutaraldehyde, 2% paraformaldehyde, and 0.1M cacodylate buffer at pH 7.4 and incubated for an overnight period at 4°C before being fixed with 1% osmium tetroxide (Merck KGaA, Darmstadt, Germany) (Sigma-Aldrich Co.). The material was then dried using propylene oxide and ethanol. The material was then sectioned (50nm) and implanted in an Agar 100 resin kit (Agar Scientific Ltd, Stansted, UK) [9].

The ultra-thin segment was stained with lead citrate and uranyl acetate before being viewed with a JEOL JEM 1010 transmission electron microscope in the Faculty of Agriculture at Mansoura University's Electron Microscopy Research Laboratory Unit.

Study of the submandibular gland homogenate's biochemistry:

Catalase, peroxidase, superoxide dismutase (SOD) and alpha-amylase were measured from SMG homogenate of all groups at the end of the study. All kits were provided by (Biodiagnostics, Giza, Egypt) and was measured by the means of (Sunostik, China).

RNA extraction and cDNA synthesis:

Total RNA extraction from tissue homogenate was performed using GENEzol ™ Reagent (Geneaid). The isolated RNA was measured using Nanodrop spectrophotometry (ND 1000-NanoDrop®). After that, cDNA was synthesized using TOPscript™ cDNA Synthesis Kit (Enzynomics). C-kit and cytokeratin-5 (CK-5) fold change expression was evaluated by real-time polymerase chain reaction using Rotor-Gene Q 2 Plex (Qiagen, Hilden, Germany). The housekeeping gene was GAPDH. The sequence of the primers is listed in table (1) [10, 11]. The relative gene expression was calculated with the $2^{\wedge-\Delta\Delta ct}$ method.

Table (1): Primer sequence of the studied genes

	Forward	Reverse
GAPDH	AATGTATCCGTTGTG GATCTGA	GCCTGCTTCACCACCT TCT
c-kit	ATCCAGCCCCACACC CTGTT	TGTAGGCAAGAACCAT CACAATGA
Cytoker atin -5	TGGTCTCCCGTGCCG CAGTTCTAT	ATTTGGGATTGG CTGTGGG

Histological study:

Light microscope study:

SMG specimens were prepared by fixing them in 10% neutral-buffered formalin, then dehydrated in progressively stronger alcohols, cleared in xylene, and then embedded in soft paraffin. Hematoxylin and eosin (H&E), Masson's trichrome stain to detect collagen fibers, and an immunohistochemical stain for S100 were used to stain sections of 5µm thickness [9].

Immunohistochemical study:
First, the SMG sections were deparaffinized, then they were rehydrated and given three PBS washes. The primary antibody (mouse monoclonal antibody to S100 protein, 1/500 dilution, clone 1A4, ab7817, Abcam) was applied to the sections and incubated overnight in a humid chamber before being rinsed three times with PBS. These sections were then three times washed in PBS after being treated for an hour with the matching biotinylated secondary antibody. To stain S100 confined structures and identify the location of immunoreactions, 3, 3'diaminobenzidine (DAB)-hydrogen peroxide was utilized as the chromogen. Finally, Mayer's hematoxylin was used to counterstain the immune-stained sections. S-100 protein antibodies are a helpful indicator of cellular damage. Normal serum was used in place of the main antibody for sections used as negative controls. Hepatic cancer served as the S100 positive control [9].

Electron microscope study:
The preparation of small gland tissue specimens for ultrastructural analysis of exosomes and alterations in SMG tissues in all analyzed groups was done as previously described.

Image analysis and morphometric studies
The Image Analyzing Unit of the Pathology Department, Faculty of Dentistry, Cairo University, Egypt, used an ordinary light microscope and a Leica 500 image analyzer computer system (England) to measure the area percent of collagen and S100 protein immune expression. Masson trichrome, S100 immunohistochemically stained sections were used for the method, which involved measuring 10 non-overlapping fields from each specimen of five randomly selected rats from each group with a total magnification of ×400.

Ethical approval:
All the experimental procedures were carried out according to the principles and guidelines of the Ethics Committee of Faculty of Medicine, Zagazig University conformed to the Guide for the care and use of Laboratory Animals, Published by US National Institutes of Health (NIH Publication No. 39/12.062022).

Statistical Analysis
SPSS (The statistical package for the social sciences) application, version 20, was used to analyze this data. Mean±Standard deviation (SD) was used to express the data collected from each group. The one-way analysis of variance (ANOVA) was used to identify a statistically significant difference (ANOVA). When P value equals 0.05, 0.001, and >0.05, an ANOVA was statistically significant, statistically extremely significant, and non-significant, respectively.

RESULTS
The biochemical, histological, immunohistochemical, and morphometrical data from each subgroup of group I were comparable. Therefore, we express the control using the results of subgroup Ia.

Characterization of Salivary Exosomes:
In TEM, salivary exosomes showed the characteristic cup-shaped spherical shape and demonstrated their size range from 30 to 150 nm (Fig. 1A). Flow cytometry analysis of salivary exosomes confirmed the positive expression of CD63 and CD9 with negative expression of 11b (Fig. 1B).

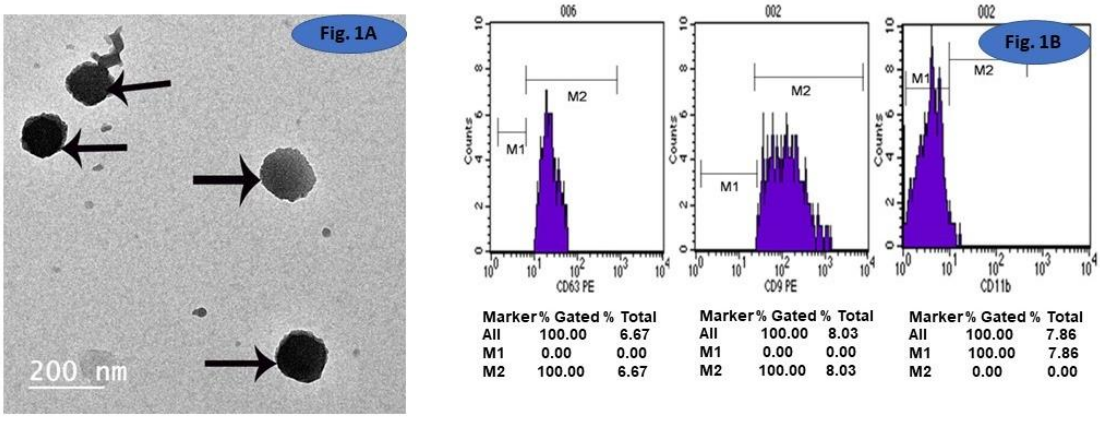

Figure (1): Characterization of Salivary Exosomes. Salivary exosomes' size and form are depicted in (A) in a TEM photomicrograph. Size varies from 30 to 150nm. (B): The positive expression of CD63 and CD9 with the negative expression of 11b was validated by flow cytometry analysis of salivary exosomes.

Biochemical results of submandibular homogenate analysis:

There was a significant decrease in the duct-ligated group compared to the control group regarding all the studied parameters. After treatment with exosomes, a significant increase in all antioxidants was recorded although it was significantly lower than in the control group **(Table 2).**

Table (2): Biochemical (antioxidants and functional) results of the studied groups:

	Control group	SMG-ligated group	Exosome-treated group
Catalase activity (U/gm tissue)	3.5±0.2	2.1±0.1*	2.8±0.2*#
Peroxidase activity (U/gm tissue)	6.7±0.5	4.3±0.2*	5.5±0.4*#
Superoxide dismutase (U/gm tissue)	1.8±0.1	0.7±0.2*	1.1±0.1*#
Amylase activity (U/mg tissue)	23.2±0.7	3.3±0.1*	6.7±0.14*#

*: a significant difference with the normal control group; #: significant difference between the ligated and treated groups.

Gene expression results:

The expression of *c-kit* was significantly elevated and *cytokeratin-5* was significantly decreased in the SMG-ligated group compared to the control. After treatment with exosomes, a significant increase in both *c-kit* and *cytokeratin-5* was recorded **(Table 3).**

Table (3): Gene expression results in the studied groups

	Control group	SMG-ligated group	Exosome-treated group
c-kit	1.01±0.2	3.62±0.5*	5.31±0.4*#
Cytokeratin-5	1.03±0.1	0.64± 0.1*	0.82±0.13*#

*: a significant difference with the normal control group; #: a significant difference between the ligated and treated groups.

Histological results:

H&E-stained sections from SMG of the control rats revealed normal histological structure of the SMG formed of lobules with closely packed serous acini and intralobular striated ducts. The acini had acidophilic cytoplasm and rounded vesicular nuclei. The striated ducts were lined by simple cuboidal epithelium with rounded nuclei and basal striations. Blood vessels between the ducts were seen **(Fig. 2A)**. Concerning SMG ligated group, it had wide spaces between the acini **(Fig. 2B)**. Acinar cells appeared with cytoplasmic vacuoles and darkly stained nuclei. Striated duct cells had cytoplasmic vacuoles and darkly stained nuclei. Thick connective tissue septa were observed **(Fig. 2 B, C & D)**. The disturbed basal cell membrane of duct cells was seen **(Fig. 2C)**. Also, thick connective tissue septa contained dilated congested blood vessels and cellular infiltration were seen **(Fig. 2D)**. Degenerated intralobular ducts appeared with vacuolated cytoplasm and darkly stained nuclei. Congested blood vessels and acini with vacuolated cytoplasm and darkly stained nuclei were seen **(Fig. 2E)**. Examination of exosome-treated group revealed an apparently normal architecture of the gland. Some duct cells still had vacuolated cytoplasm and darkly stained nuclei **(Fig. 2F)**.

Masson trichrome-stained sections of SMG of control rats showed scanty collagen fibers in the connective tissue septa between the lobules of the gland and surrounding both acini and ducts **(Fig. 3A)**. While, SMG-ligated group revealed deposition of abundant amount of collagen fibers in the capsule and connective tissue septa **(Fig. 3B)**. In exosome-treated group, collagen fibers decreased compared to SMG ligated group **(Fig. 3C)**. Statistical results of mean area percentage of collagen fibers confirmed previous results **(Fig. 3D)**.

S100 immuno-stained sections of the SMG of the control rats showed weak positive S100 immunoreaction in the cytoplasm of a few duct cells and cells surrounding the acini **(Fig. 4A)**. SMG-ligated group revealed strong positive S100 immunoreaction in the cytoplasm and nuclei of nearly all duct epithelial cells and cells surrounding the acini **(Fig. 4B)**. In exosome-treated group, S100 immunoreaction decreased compared to SMG-ligated group **(Fig. 4C)**. Statistical results of mean area percentage of S100 immunoreaction confirmed previous results **(Fig. 4D)**.

Examination of TEM sections of the SMG of the control group showed acinar cells with numerous electron-dense secretory granules of variable sizes filling the cytoplasm and basal euchromatic rounded nuclei with prominent nucleoli**.** Packed parallel cisternae of RER, mitochondria and intact intercellular junction could be seen **(Fig. 5A & B)**. SMG-ligated group showed acinar cells with condensed heterochromatic nuclei, fused secretory granules of variable sizes and densities, cytoplasmic vacuolations and dilated RER. Wide intercellular spaces with disrupted microvilli and many collagen fibers were observed **(Fig. 5C)**. While, exosome-treated group demonstrated apparently normal acinar cells **(Fig. 5D)**.

TEM sections of the SMG of the control group showed striated duct cells surrounding the regular lumen with basal rounded euchromatic nuclei. The cytoplasm of duct cells contained multiple apical electron-dense granules**,** numerous mitochondria and basal striations **(Fig.6A)**. In SMG-ligated group, striated duct cells revealed irregular heterochromatic nuclei, few apical small electron-dense granules and cytoplasmic vacuolations. Wide intercellular spaces and disrupted basal striations were seen. Some cells appeared with rarified cytoplasm, mitochondria with disrupted crista. Many collagen fibers and irregular lumen were observed **(Fig. 6B & C)**. Examination of exosome-treated group revealed apparently normal duct cells **(Fig. 6D)**.

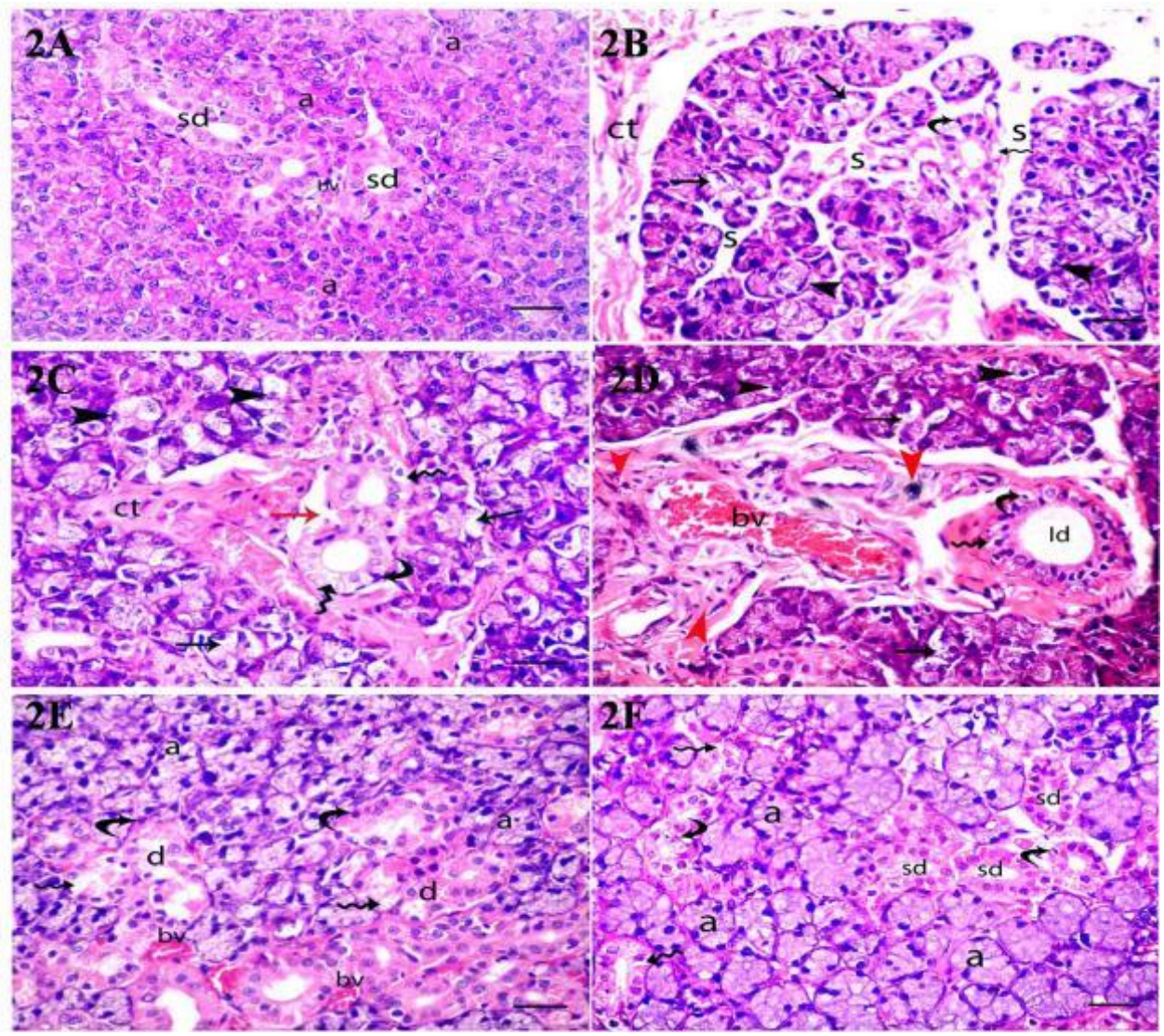

Figure (2): H&E-stained sections of the SMG of the study groups. **[A]** Control. **[A]**Showing lobules containing closely packed serous acini and intralobular striated ducts. The acini **(a)** have acidophilic cytoplasm and rounded vesicular nuclei. The striated ducts **(sd)** are lined by simple cuboidal epithelium with rounded nuclei and basal striations. Blood vessels **(bv)** between the ducts are seen. **[B-E]** SMG-ligated group. **[B]**Wide spaces **(s)** between the acini and acinar cells appear with cytoplasmic vacuoles **(arrow)** and darkly stained nuclei **(arrowhead)**. Striated ducts have cytoplasmic vacuoles **(wavy arrow)** and dark stained nuclei **(curved arrow)**. Thick connective tissue **(ct)** can be seen. **[C]** Acinar cells appear with cytoplasmic vacuoles **(arrow**) and darkly stained nuclei **(arrowhead)**. The cells lining striated ducts show cytoplasmic vacuoles **(wavy arrow),** darkly stained nuclei **(curved arrow),** and disturbed basal cell membrane (**red arrow)**. Thick connective tissue septa **(ct)** are observed. **[D]** Showing thick connective tissue septa with dilated congested blood vessels **(bv)**, and cellular infiltration **(red arrowhead)**. Interlobular ducts **(Id)** appear with vacuolated cytoplasm **(wavy arrow)** and dark nuclei **(curved arrow)**. Acinar cells with vacuolated cytoplasm **(arrow)** and darkly stained nuclei **(arrowhead)** are also seen. **[E]** Degenerated intralobular ducts **(d)** with vacuolated cytoplasm **(wavy arrow)** and darkly stained nuclei **(curved arrow)** are observed. Congested vessels **(bv)** and acini **(a)** with vacuolated cytoplasm and darkly stained nuclei are seen. **[F]** Exosome-treated. **[F]**An apparently normal architecture of the gland formed of closely packed acini **(a)**, and striated ducts **(Sd)**. Some duct cells still have vacuolated cytoplasm **(wavy arrow)** and darkly stained nuclei **(curved arrow)**. **(H & E X 400 scale bar 20 um)**.

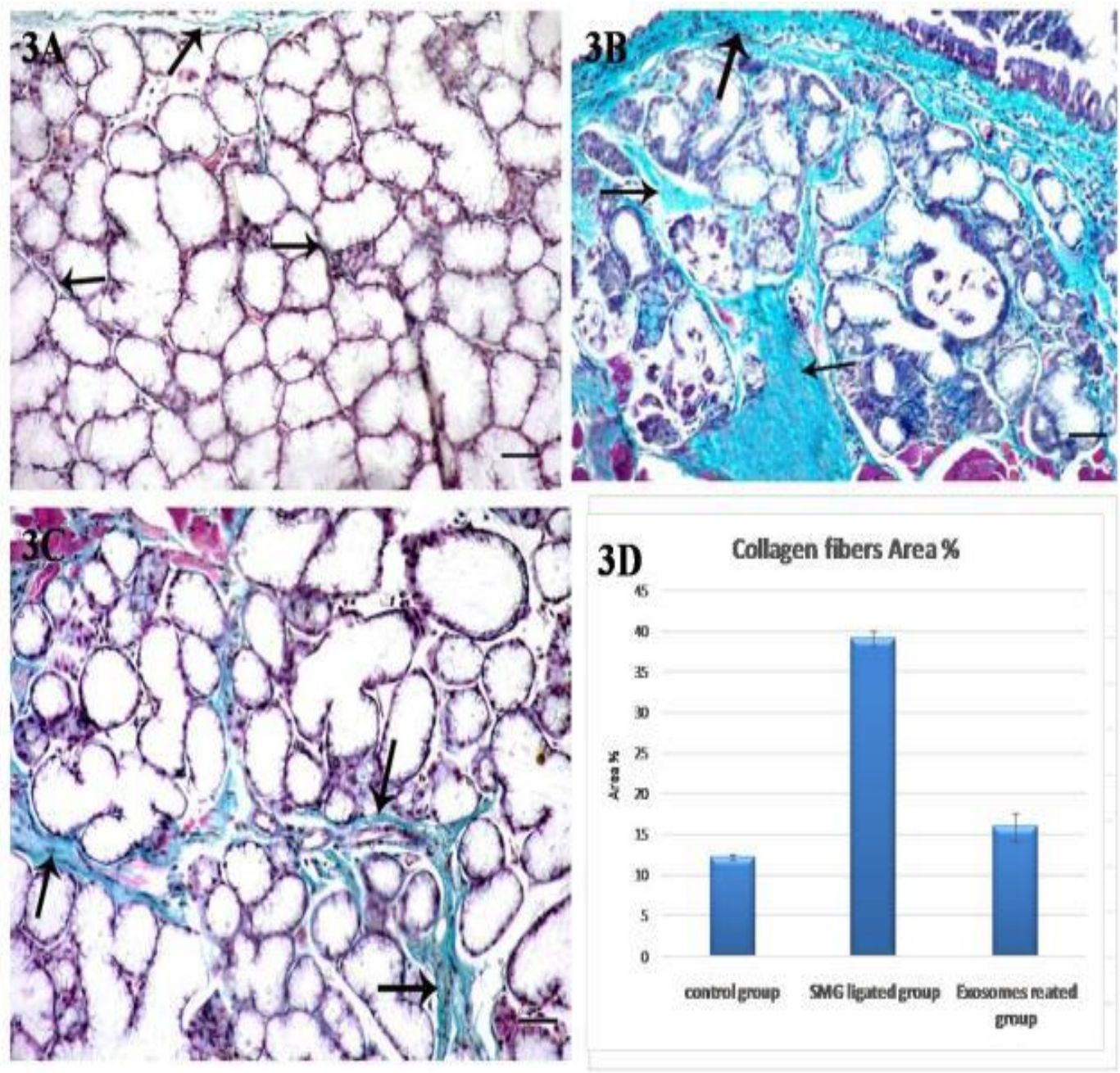

Figure (3): Masson trichrome-stained sections of the SMG of the study groups. **[A]** Control group reveals scanty collagen fibers **(arrows)** in the connective tissue septa between the lobules of the gland and surrounding both acini and ducts. **[B]**SMG-ligated group shows deposition of abundant collagen fibers **(arrows)** in the capsule, connective tissue septa between the lobules that extend to surround the acini and ducts. **[C]**Exosome-treated group reveals decreased collagen fibers **(arrow)** in connective tissue septa in comparison to group II **(Masson trichrome, X 200 scale bar 30um)**. **[D]**Bar chart of mean area % of collagen fibers shows a statistically significant increase among SMG ligated group compared to control and exosome-treated groups. No significant difference is found between the control and exosome-treated groups.

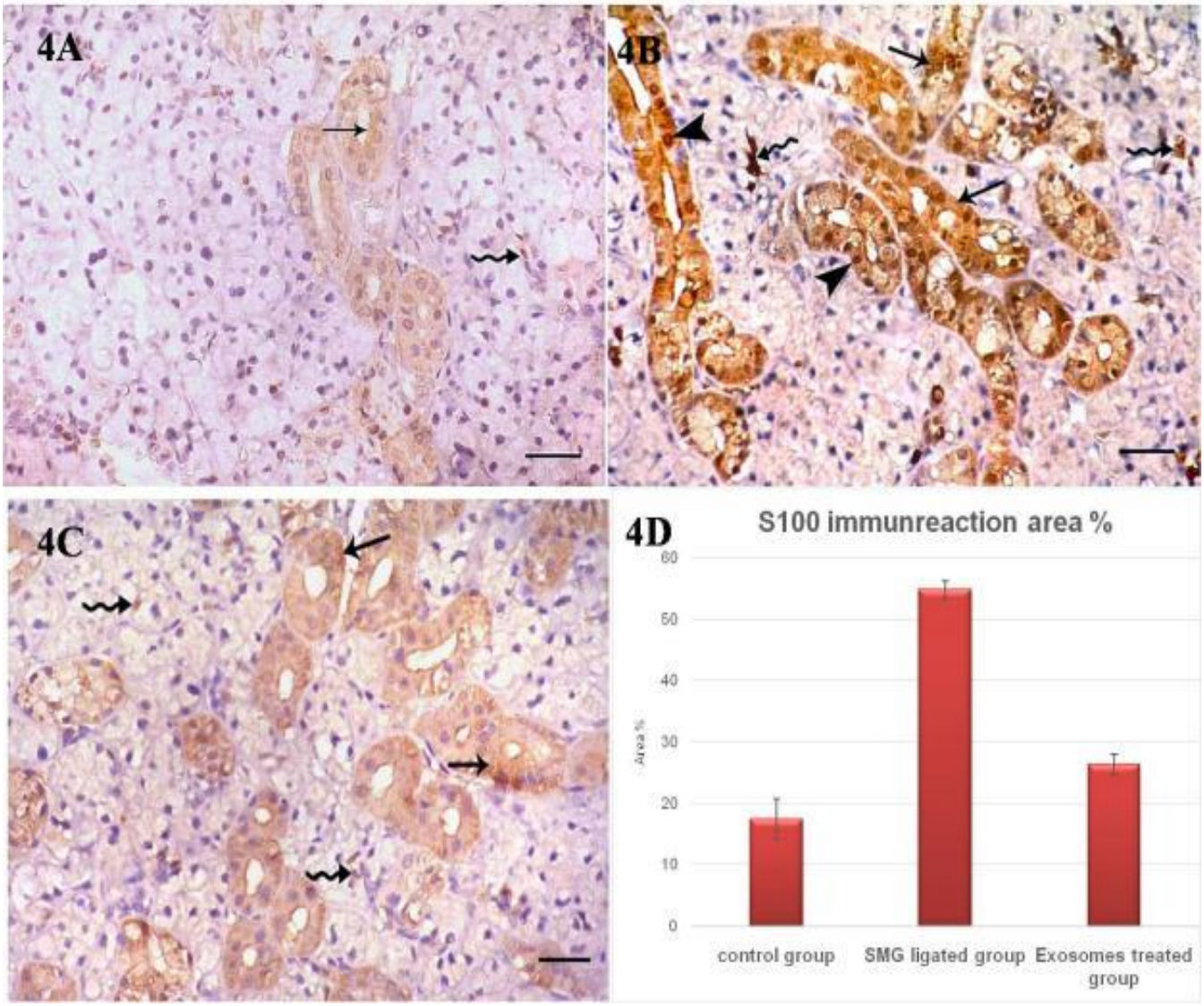

Figure (4): S100 immuno-stained sections of the SMG of the study groups. **[A]**Control group shows weak positive S100 immunoreaction in the cytoplasm **(arrow)** of a few duct cells and cells surrounding the acini **(wavy arrow)**. **[B]** SMG-ligated group reveals strong positive S100 immunoreaction in the cytoplasm **(arrow)** and nuclei **(arrowhead)** of nearly all duct epithelial cells and cells surrounding the acini **(wavy arrow). [C]**Exosome-treated group shows decreased S100 immunoreaction in the cytoplasm **(arrow)** of duct cells and cells surrounding the acini **(wavy arrow)** in comparison to group II **(S100 immunoreaction X 400 scale bar 20um). [D]** Bar chart of mean area % of S100 immunoreaction shows a statistically significant increase in SMG-ligated group compared to the control and exosome-treated groups. No significant difference is found between control and exosome-treated groups.

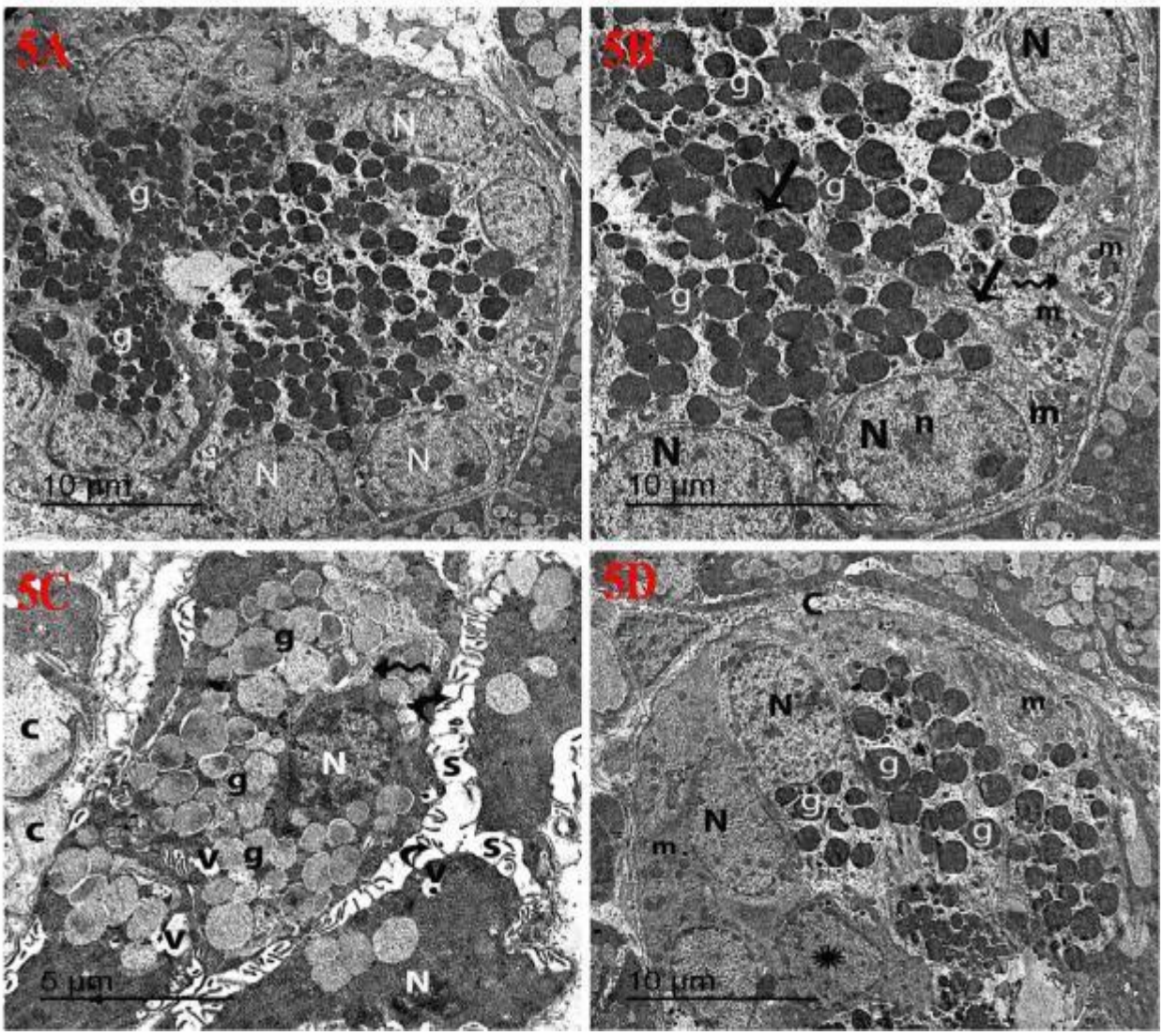

Fig. (5): TEM of the SMG from all the study groups. **[A and B]** Control group. **[A]**Acinar cells have numerous electron-dense secretory granules **(g)** of variable sizes filling the cytoplasm and basal euchromatic rounded nuclei **(N)**. **[B]** Higher magnification of acinar cells shows numerous electron-dense secretory granules **(g)** of variable sizes, euchromatic nuclei **(N)** with prominent nucleoli**(n)**, packed parallel cisternae of RER **(wavy arrow),** and mitochondria **(m)**. An intact intercellular junction **(arrows)** can be seen. **[C]**SMG-ligated group. **[C]** Acinar cells appear with condensed heterochromatic nuclei **(N)**, fused secretory granules **(g)** of variable sizes and densities and cytoplasmic vacuolations **(v)**. Dilated RER **(wavy arrow)** can be seen. Wide intercellular spaces **(S)** with disrupted microvilli **(curved arrow)** and many collagen fibers **(C)** are observed. **[D]**Exosome-treated group. **[D]** Some acinar cells appear with euchromatic nuclei **(N),** numerous electron dense secretory granules **(g)** of variable sizes filling the cytoplasm. Other acinar cells have nuclei **(asterix)** with peripheral clumps of heterochromatin. Mitochondria **(m)** and a few collagen fibers **(C)** are observed.

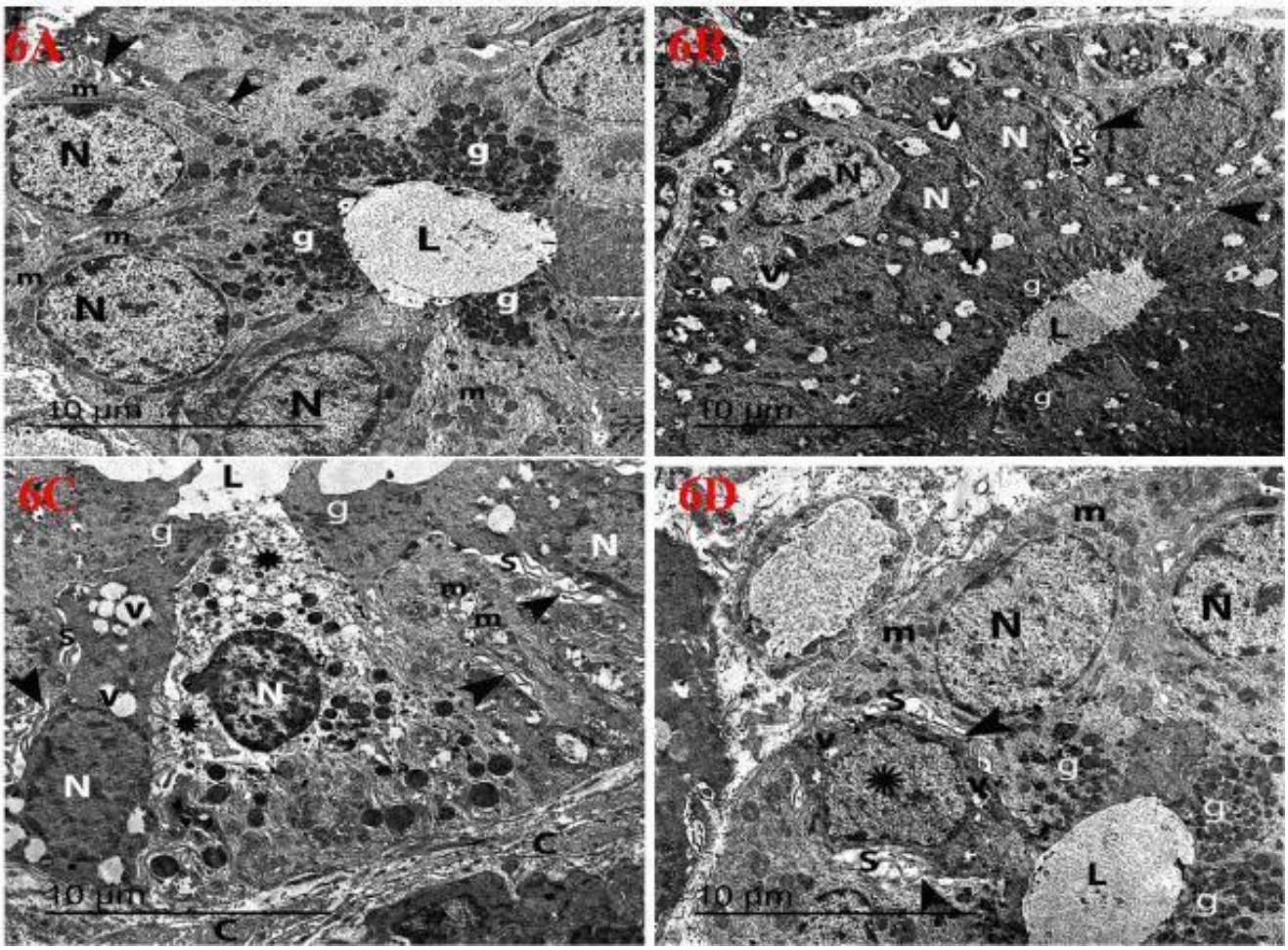

Fig. (6): TEM of the SMG from all the study groups. **[A]** Control group, of striated duct cells are surrounding a regular lumen **(L)** with basal rounded euchromatic nuclei **(N)**. The cytoplasm of duct cells contains multiple apical electron-dense granules **(g),** and numerous mitochondria **(m**). Basal striations **(arrowheads)** can be seen. **[B and C]** SMG-ligated group. **[B]** Striated duct cells show irregular heterochromatic nuclei **(N)**, few apical small electron dense granules **(g),** and cytoplasmic vacuolations **(v)**. Wide intercellular spaces **(s**) and disrupted basal striations **(arrowhead**) are seen. Lumen **(L)** filled with secretions are observed. **[C]** A higher magnification of some lining cells of striated duct appear with heterochromatic nuclei **(N)**, cytoplasmic vacuolations **(V)**, and few apical small electron-dense secretory granules **(g)**. Some cells appear with rarified cytoplasm **(asterix)**. Mitochondria **(m)** with disrupted crista, wide intercellular spaces **(S)** and disrupted basal striations **(arrow head)** can be seen. Many collagen fibers **(C)** and irregular lumen **(L)** are also observed. **[D]** Exosomes treated group. [D] Some duct cells appear with basal euchromatic nuclei **(N)**, multiple apical electron-dense granules **(g)** and numerous mitochondria **(m)**. While; other duct cells have an irregular heterochromatic nucleus **(asterix)**, wide intercellular spaces **(S)** with disrupted basal satiations **(arrowhead)** and cytoplasmic vacuolations **(v).**

Morphometrical and statistical results:

There was a statistically significant difference between the study groups in area % of both collagen fibers and S100 immunoreaction. Post hoc test showed that there was a statistically significant increase in both among SMG-ligated group compared to control and exosome-treated groups. No difference was found between the control and exosome-treated groups (**Table 4).**

Table (4): Mean surface area percentage (%) of collagen fibers deposition and S100 immunoreaction area % in the study groups

Variable	Control group n=24	SMG-ligated group n=8	Exosome-treated group n=8	F	P	Post hoc
Collagen fibers (area %)	12.20±0.3	39.10±0.9	15.94±1.7	**2909**	**<0.001****	**<0.001**[1]** 0.87 NS[2] **<0.001**[3]**
S100 *immunoreaction* (area %)	17.50±3.21	54.77±1.5	26.33±1.7	564.9	**<0.001****	**<0.001**[1]** 0.81 NS[2] **0.002*[3]**

Data presented as mean ($\bar{x}$) ± standard deviation (SD), F: ANOVA test.
NS: Non significant (P>0.05) *: Significant (P<0.05) **: Highly significant (p<0.001)
Post hoc: P1: Group I versus II P2: Group I versus III P3: Group II versus III

DISCUSSION

Obstruction of the salivary glands affects their function. It decreases the flow of saliva and changes its composition, disturbing oral health. To restore salivary functions after radiation or mechanical injuries, a precise explanation of the biochemical mechanisms involved in the functional improvement of the glands would be required [7, 12].

In the current study, we used the extra-oral route of SMG ligation in rats for duct occlusion because it is practical and repeatable [7,13]. Due to their histo-morphological parallels to humans and experimental conveniences [12], Rats models were chosen as experimental animals.

Although exosomes are a novel and highly promising medication delivery mechanism, there are few studies on how they treat xerostomia and salivary gland disorders.

Our findings in the current study are consistent with those of other earlier studies that found salivary exosomes to be spherical, cup-shaped vesicles with a size range of 30-150 nm with positive CD9 and CD63 expression [14].

Starch is transformed into smaller sugar molecules by salivary amylase to be taken into the bloodstream. Thus, blood glucose is dysregulated by gland blockage. Salivary amylase also breaks down various insoluble polysaccharides into smaller soluble components. Therefore, it is essential to remove food after chewing in order to wipe out the components required for microbial growth [11].

After SMG duct ligation, a substantial decrease in amylase output was seen in our study. Similar to our findings, it was discovered that unilateral parotid gland duct ligation dramatically decreased amylase activity. The decrease in content in the parotid homogenate, rather than a change in the secretory pathway, accounted for this drop in activity [15].

After SMG duct ligation in our study, peroxidase activity dramatically decreased. This result was consistent with past findings. Peroxidase activity dropped to 30% of control gland activity by the second day of ligation and remained there through the remainder of the study [16].

Regarding catalase and SOD, there was a significant decrease in their activities after duct ligation. Similarly, an oxidative stress state caused a decrease in glutathione peroxidase and SOD accompanied by a rise in reduced glutathione and inducible nitric oxide synthase. This imbalance results in cell damage [17].

After salivary exosomes injection in our study, a significant increase in antioxidant activity was recorded. Similarly, it was found that cells treated with stem cells derived-exosomes displayed a decrease in ROS generation and oxidative stress. This was explained by the presence of anti-oxidant molecules like catalase and SOD in those tissues [18].

Cytokeratin-5 (CK-5) is an epithelial basal cell protein, it is an exocrine gland stem cell marker. Also, it is an acinar cell precursor gene marker [19]. Our study detected that *CK-5* expression significantly decreased after ligation. The same result was found by **Wang *et al.*** [20], additionally, they discovered enhanced *CK-5* expression following release of ligation, indicating that atrophic salivary glands may be capable of regeneration following recovery from long-term blockage [20]. Also, **Watanabe *et al.*** [13] found a significant steady increase in *CK-5* expression two months after the removal of the obstruction. After treatment with exosomes, a significant increase of *CK-5* expression was recorded. This finding demonstrates

that salivary exosomes can promote the differentiation of precursor cells in atrophic salivary glands.

In our study, there was a significant elevation in *c-kit* expression after duct ligation. This result was similar to that found by **Wang *et al.*** [20]. They discovered that 2 months after ligation, c-kit expression was increased. C-kit expression continued to significantly rise after exosome delivery. While C-kit suppression causes cell death, activation promotes mitosis and inhibits apoptosis. Additionally, **Watanabe *et al.*** [13] claimed that cells that express the c-kit are capable of regenerating glands.

In the current study, the control group displayed nearly normal histological appearance for all subgroups. These results were in the same line with **Woods *et al.*** [7].

In the present study, H&E-stained sections from the SMG-ligated group demonstrated degenerative lesions in the form of wide spaces between the acini, vacuolated cytoplasm, darkly stained nuclei, congested blood vessels, cellular infiltration, and disturbed basal cell membrane of interlobular ducts. The same results were established by **Scott *et al.*** [21]**.** They found that the parotid gland's obstructed ducts underwent atrophy, losing over 85% of its parenchyma. They explained these outcomes by the direct injury by back-pressure of the excretory duct contents which was followed by inflammatory alterations and additional cell damage and atrophy.

The apoptotic response occurred in all of the acinar cells a few days after the blockage, and the apoptotic cells were then phagocytosed by the surrounding acinar cells or intraepithelial macrophages, according to a previous work by **Takahashi *et al.*** [22]. Furthermore, **Osailan *et al.*** [16] attributed these atrophic modifications to disuse atrophy, wherein the restriction of secretion resulted in the internal cellular dismantling of stored granules with subsequent acinar and glandular atrophy.

Also, **Silver *et al.*** [23] attributed these findings to mTOR pathway activation and upregulation of autophagy-related proteins**.** In addition, **Buyuk *et al.*** [17] noted that under an oxidative stress state, there was an imbalance between oxidants and antioxidants resulting in cell damage. Furthermore, **Ekaluo *et al.*** [24] explained how oxidative stress affects the SMG's secretory function and secretory protein synthesis. As a result, secretory material builds up in the cytoplasm of acinar cells, resulting in cellular atrophy and ultimately death.

In the current work, cytoplasmic vacuolization's were found by LM and TEM in both acini and ducts of SMGs. It was described by **Hishida *et al.*** [25] who revealed that cytoplasmic vacuoles first developed in SMG tissue after duct ligation. They stated that some of these vacuoles were neutral fat droplets and may have been involved in the necrosis and cell death process**.** Another study suggested that damaged organelles like mitochondria and lysosomes or autophagic vacuoles could cause vacuolations under EM [26].

The current study's findings about the apoptotic response by both LM and TEM as dark stained, and irregular heterochromatic nuclei following duct obstruction are consistent with **Maria *et al.*** [27] who showed the apoptotic response in ductal cells following parotid duct ligation. They linked this to the disturbance in membrane receptors and signaling pathway of acinar cells**.** Also, **Eldahrawy *et al.*** [28] documented that the nucleus acquired irregular forms to increase the surface area of contact with the cytoplasm as a compensatory mechanism for reduced metabolic activity due to apoptosis**.**

Concerning congested blood vessels and extravasation of red blood cells (RBCs) in the present study, they were in consistent with **Mubarak** [29], who explained that intolerable inflammation may cause a microcirculatory disturbance and complete loss of capillary integrity, which may result in hemorrhage and increase the amount of blood flow to the degenerating areas of the SMG. Moreover, **Elsakhawy *et al.*** [30] found that the interacinar blood capillaries in SMG were congested. Additionally, the blood vessels in the connective tissue surrounding the interlobular ducts were dilated and visibly engorged.

Our findings regarding cellular infiltration were consistent with those of **Woods *et al.*** [7]**,** who stated that after SMG duct ligation, there was neutrophil, monocyte, macrophage, and T-cell infiltration as well as the generation of inflammation, both of which are probably responsible for SMG degeneration.

TEM examination of the SMG ligated group revealed dilated RER and mitochondria with disrupted crista. According to **Bredholt *et al.*** [31], dilated and disordered RER may indicate cell damage rather than an increase in secretory activity. The expansion in RER may be a sign of problems with the exocytosis of secretory material or it may be a sign of reversible cell damage that causes secretory material to build up inside cisternae**.** Additionally, **Hidayat *et al.*** [32] hypothesized that mitochondrial damage may be related to the cytotoxic property of reactive oxygen species (ROS) that destroys mitochondrial DNA, limiting mitochondrial metabolism.

In the current research, collagen fibers deposition was statistically significantly higher in the area percentage of the SMG ligated group in Masson trichrome stained sections. This result was consistent with that of **Woods *et al.*** [7]**,** who discovered that following ligating the SMG in mice, there was a rise in collagen fiber deposition and glandular atrophy. They explained this result as being caused by the SMG's overexpression of TGF-β and its receptors. TGF-β promotes the production of collagen and fibronectin, two essential proteins in the progression of fibrosis.

In the current work, S100 immuno-stained sections of SMG of the control group revealed weak positive reactions in the cytoplasm of duct cells and cells surrounding the acini. This finding was in line with **Elsharkawy and Alhazzazi** [6] who revealed weak staining of the S100 protein in myoepithelial cells, secretory portions, granular convoluted tubules and striated ducts of normal SMG.

The SMG-ligated group demonstrated a statistically significant increase in the area% of S100 immuno-stained reactions. S100 proteins can be produced extracellularly in response to stimuli or cell damage. Additionally, they improve apoptosis, inflammation, cell proliferation, and survival as well as the survival and extension of neurons [6].

Also, antibodies to the S100 protein could be employed as a helpful indicator of cellular damage in the salivary glands following treatment with two different doses of the antidepressant drug amitriptyline **[6].** Furthermore, the S100 protein was largely identified in bile duct epithelial cells and its expression increased proportionally to the ductular response during fibrogenesis by bile duct ligation. As S100 controls hepatic stellate cells activation-related fibrotic proteins via RAGE, they claimed that upregulated S100 has a possible role in the progression of liver fibrosis **[33]**. This also may explain why fibrosis occurred in the current study.

Regarding the exosomes-treated group, there was an amelioration in the morphological and biochemical changes detected in the SMG-ligated group. These results were consistent with **Wu *et al.*** **[34]** who postulated that the miRNAs of exosomes were crucial regulators of cell cycle progression, proliferation, and modulating angiogenesis and inflammation**.** Also, **AbuBakr *et al*.** **[35]** found promising improvements in the ultrastructural findings after the treatment with exosomes in the glandular and ductal components with diminished fibrosis**.** This was explained by inhibiting TGF-β pathway via Smad2 and Smad3.

CONCLUSION AND RECOMMENDATION

There were improved histological, immunohistochemical and biochemical alterations after treatment with salivary exosomes. So, salivary exosomes could be a possible modality in treating SMG diseases. It is recommended to be applied in future clinical applications for treating several diseases. Finally, more studies are required to ensure the safety of salivary exosome injection on the long-term.

Acknowledgment: None.

Conflict of Interest: None

Funding sources: None.

REFERENCES

1. **Desoutter A, Soudain-Pineau M, Munsch F *et al.* (2012):** Xerostomia and medication: a cross-sectional study in long-term geriatric wards. The Journal of Nutrition, Health & Aging, 16(6): 575-579.
2. **Carlson E, Ord R (2015):** Trauma and Injuries to the Salivary Glands. Salivary Gland Pathology: Diagnosis and Management, Pp. 409-436. https://onlinelibrary.wiley.com/doi/book/10.1002/9781118949139
3. **Akadomari K, Tanaka A, Mataga I (2016):** Regenerative capacity of atrophic submandibular gland by duct ligation in mice. Journal of Hard Tissue Biology, 25(2): 121-130.
4. **Chuo S, Chien J, Lai C (2018):** Imaging extracellular vesicles: Current and emerging methods. J. Biomed. Sci., 25: 1-10.
5. **Chen Y, Lin E, Chiou T *et al.* (2020):** Exosomes in clinical trial and their production in compliance with good manufacturing practice. Tzu-Chi Medical Journal, 32(2): 113.-120.
6. **Elsharkawy G, Alhazzazi T (2016):** The effect of the commonly used antidepressant drug amitriptyline (TCAs) on the salivary glands. J Dent. Oral Disord. Ther., 4(4): 1-5
7. **Woods L, Camden J, El-Sayed F *et al.* (2015):** Increased expression of TGF-β signaling components in a mouse model of fibrosis induced by submandibular gland duct ligation. PLoS One, 10(5): e0123641. https://doi.org/10.1371/journal.pone.0123641
8. **Ebrahim N, Ahmed I, Hussien N *et al.* (2018):** Mesenchymal stem cell-derived exosomes ameliorated diabetic nephropathy by autophagy induction through the mTOR signaling pathway. Cells, 7(12): 226. doi: 10.3390/cells7120226.
9. **Suvana S, Layton C, Bancroft J (2019):** Bancroft's theory and practice of histological techniques. 8th ed, New York, London: Churchill Livingstone. https://www.us.elsevierhealth.com/bancrofts-theory-and-practice-of-histological-techniques-9780702068645.html
10. **Barlow N, Phillips S, Wallace D *et al.* (2003):** Quantitative changes in gene expression in fetal rat testes following exposure to di(n-butyl) phthalate. Toxicol. Sci., 73(2): 431-341.
11. **El Sadik A, Mohamed E, El Zainy A (2018):** Postnatal changes in the development of rat submandibular glands in offspring of diabetic mothers: Biochemical, histological and ultrastructural study. PLoS One, 13(10): e0205372. doi: 10.1371/journal.pone.0205372.
12. **Maruyama C, Monroe M, Hunt J *et al.* (2019):** Comparing human and mouse salivary glands: A practice guide for salivary researchers. Oral Diseases, 25(2): 403-415.
13. **Watanabe H, Takahashi H, Hata-Kawakami M *et al.* (2017):** Expression of c-kit and Cytokeratin 5 in the submandibular gland after release of long-term ligation of the main excretory duct in mice. Acta Histochemica et Cytochemica, 50(3): 111-118.
14. **Zlotogorski-Hurvitz A, Dayan D, Chaushu G *et al.* (2015):** Human saliva-derived exosomes: comparing methods of isolation. Journal of Histochemistry & Cytochemistry, 63(3): 181-189.

15. **Nemoto-Murata K (1986):** Effect of duct ligation on amylase release from rat parotid slices. Jpn. J. Pharmacol., 41(1):33-38.
16. **Osailan S, Proctor G, McGurk M *et al.* (2006):** Intraoral duct ligation without inclusion of the parasympathetic nerve supply induces rat submandibular gland atrophy. International Journal of Experimental Pathology, 87(1): 41-48.
17. **Buyuk B, Parlak S, Keles O *et al.* (2015):** Effects of diabetes on post-Menopausal rat submandibular Glands: A Histopathological and Stereological Examination. Eurasian J. Med., 47(3): 199-207.
18. **Bodega G, Alique M, Puebla L *et al.* (2019):** Microvesicles: ROS scavengers and ROS producers. J. Extracell Vesicles, 8(1):1626654. doi: 10.1080/20013078.2019.1626654.
19. **Murayama K, Kawakami M, Tanaka A (2017):** Chronic changes in the atrophied submandibular gland after long-term ligation of the main excretory duct in mice. J. Hard Tissue Biol., 26: 13–22.
20. **Wang X, Qi S, Wang J *et al.* (2014):** Spatial and temporal expression of c-Kit in the development of themurine submandibular gland. J. Mol. Histol., 45: 381–389.
21. **Scott J, Liu P, Smith P (1999):** Morphological and functional characteristics of acinar atrophy and recovery in the duct-ligated parotid gland of the rat. Journal of Dental Research, 78(11): 1711-1719.
22. **Takahashi S, Nakamura S, Suzuki R *et al.* (2000):** Apoptosis and mitosis of parenchymal cells in the duct-ligated rat submandibular gland. Tissue and Cell, 32(6): 457-463.
23. **Silver N, Proctor G, Arno M *et al.* (2010):** Activation of mTOR coincides with autophagy during ligation-induced atrophy in the rat submandibular gland. Cell Death Dis., 1(1): 14-10.
24. **Ekaluo U, Uno U, Edu N *et al.* (2016):** Effect of Trévo dietary supplement on caffeine induced Oxidative Stress in Albino Rat Models. The Pharmaceutical and Chemical Journal, 3(2):92-97.
25. **Hishida S, Ozaki N, Honda T *et al.* (2016):** Atrophy of submandibular gland by the duct ligation and a blockade of SP receptor in rats. Nagoya J. Med. Sci., 78(2):215–227.
26. **Singh A, Singh O (2016):** Ultrastructural changes in the sublingual salivary gland of prenatal buffalo (Bubalus bubalis). Veterinary World, 9(3): 326-29.
27. **Maria O, Maria S, Redman R *et al.* (2014):** Effects of double ligation of Stensen's duct on the Rabbit Parotid Gland. Biotech. Histochem., 89: 181–198.
28. **Eldahrawy D, Adawy H, El Deeb M (2022):** The effect of bone marrow derived mesenchymal stem cells on the ultrastructure of submandibular salivary gland of induced hypothyroidism in rats (Electron Microscopic Study). Egyptian Journal of Histology, 45(2): 472-490.
29. **Mubarak R (2012):** Effect of red bull energy drink on rats submandibular salivary glands (light and electron microscopic study). J. Am. Sci., 8(1): 366-372.
30. **ElSakhawy M, Mohamed D, Ahmed Y (2019):** Histological and immunohistochemical evaluation of the effect of tartrazine on the cerebellum, submandibular glands, and kidneys of adult male albino rats. Environmental Science and Pollution Research, 26(10): 9574-9584.
31. **Bredholt T, Dimba E, Hagland H *et al.* (2009):** Camptothecin and khat (*Catha edulis* Forsk.) induced distinct cell death phenotypes involving modulation of c-FLIPL, Mcl-1, procaspase-8 and mitochondrial function in acute myeloid leukemia cell lines. Molecular Cancer, 8: 1–13.
32. **Hidayat M, Khaliq S, Khurram A *et al.* (2019):** Protective effects of melatonin on mitochondrial injury and neonatal neuron apoptosis induced by maternal hypothyroidism. Melatonin Research, 2(4): 42-60.
33. **Park J, Kim M, Kim S et al. (2021):** Increased expression of S100B and RAGE in a mouse model of bile duct ligation-induced liver fibrosis. Journal of Korean Medical Science, 36(14): 90. doi: 10.3346/jkms.2021.36.e90
34. **Wu J, Wang Y, Li L (2017):** Functional significance of exosomes applied in sepsis: a novel approach to therapy. BBA Mol. Basis Dis., 1863(1):292-297.
35. **AbuBakr N, Haggag T, Sabry D *et al.* (2020):** Functional and histological evaluation of bone marrow stem cell-derived exosomes therapy on the submandibular salivary gland of diabetic Albino rats through TGFβ/ Smad3 signaling pathway. Heliyon., 6(4):e03789. doi: 10.1016/j.heliyon.2020.e03789.